Pol. J. Environ. Stud. Vol. XX, No. X (XXXX), 1-12
DOI: *10.15244/pjoes/195347* ONLINE PUBLICATION DATE:

Original Research

Attenuation of Phosphate and Fluoride from Phosphogypsum Leachate by Rice Husk Biochar

Xin Peng[1,2,3], Yinger Deng[4], Jie Zhang[5], Shuai Gao[1], Yunfeng Zhang[1]*, Shanming Wei[1], Zhetong Liu[1], Bo Zhou[1]

[1]Shandong Provincial Geo-mineral Engineering Exploration Institute, Shandong Provincial Bureau of Geology & Mineral Resources, Shandong Engineering Research Center for Environmental Protection and Remediation on Groundwater, Jinan 250014, P. R. China
[2]Sichuan Provincial Engineering Research Center of City Solid Waste Energy and Building Materials Conversion and Utilization Technology, Chengdu University, Chengdu 610106, P. R. China
[3]School of Architecture and Civil Engineering, Chengdu University, Chengdu 610106, P. R. China
[4]College of Environment and Civil Engineering, Chengdu University of Technology, Chengdu 610059, P. R. China
[5]Central & Southern China Municipal Engineering Design and Research Institute Co., Ltd, WuHan 430010, P. R. China

Received: 11 July 2024
Accepted: 28 October 2024

Abstract

The massive accumulation of phosphogypsum (PG) in the open air can produce a large quantity of phosphorus- (P) and fluoride- (F) rich acidic solution, which is environmentally and ecologically dangerous. However, very few studies have focused on this serious issue. In this regard, batch experiments were conducted to test the adsorption characteristics and capacity of rice husk biochar (RHB) pyrolyzed at 600 °C for P and F from real PG leachate. The results indicated good adsorption capacity (3838 mg-P/kg and 2500 mg-F/kg), which was mainly controlled by electrostatic attraction and precipitation mechanisms. The column-packed RHB at a dosage of 93 g and an influent flow rate of 0.5 ml/min was the best for the P and F removal from real PG leachate. Various breakthrough curve models were used to simulate the experimental data, and the model fitting results revealed that all models except the Adams-Bohart model well simulated the dynamic adsorption behaviors of P and F. The BDST model results show that RHB can be a low-cost, safe, reliable adsorbent in real-world applications to remove P and F from PG leachate.

Keywords: highly acidic, eutrophication, leachate treatment, effectiveness, low cost

Introduction

Phosphogypsum (PG) is a byproduct of the production of phosphate plant fertilizer, and phosphoric acid is used in the wet acid processing of phosphate rock ore. It is estimated that 4–6 tons of PG are typically generated per ton of phosphoric acid [1]. The phosphate and fluoride contents were 0.5~2.5%, which is generally higher than the contents of other impurities in PG [2]. However, most studies focused on analyzing the concentration and behavior of metals and radionuclides, and phosphate and fluoride are often

*e-mail: zhangyunfengSD@126.com

neglected. Phosphorous (P) has been widely considered the dominant driver of eutrophication [3]. Excessive P can trigger harmful algal blooms, which can severely degrade the inland and coastal water quality [4]. In fact, the Yangtze River, which is the largest river in China, became the river with the most exceeded standard P index in 2016 [5]. PG storage piles in the upper reaches of the Yangtze River Basin play an important role in the release of P [6]. In addition, drinking water is the most important exposure pathway through which fluoride enters the human body [7]. Previous studies have shown that limited concentrations of fluoride in drinking water can prevent dental caries and exert beneficial effects on bone strength [8]. However, chronic exposure to high fluoride concentrations in drinking water can induce skeletal fluorosis and cancer [9]. Leachates from unlined PG storage piles directly infiltrate groundwater and threaten both ecological safety and human health. Therefore, there is an urgent need to develop feasible and effective techniques to treat leachates from older, unlined PG storage piles to benefit the local hydrology and ecology and protect potable water resources. Several studies attempted to determine the influence of the efflux of contaminants from PG leaching, which are mainly heavy metals and radioactive pollutants, on the surrounding environment [10-11]. However, few studies focused on the treatment of PG leachates at disposal sites. Millán-Becerro et al. used passive treatment systems with dispersed alkaline substrates (e.g., limestone, barium carbonate, and calcium hydroxide) to treat PG leachates [12]. The alkaline substrate efficiently removed heavy metals, phosphate, and fluoride, mainly through phosphate precipitation.

Biochar was recently used to significantly advance the removal of different pollutants from aqueous solutions and is considered an efficient, low-cost, and eco-friendly ameliorant in water [13-14]. Moreover, the alkalinity of biochar can neutralize the acid from leachate, which may contribute to the formation of precipitates on the biochar surface. The high specific surface area of biochar can provide more adsorption sites and may contribute to the adsorption of P and F by electrostatic attraction. The well-developed pore structure of biochar can increase the number of permeability channels to help prevent typical clogging problems that are associated with Ca and Mg precipitation [15]. Therefore, biochar can provide easier and less expensive treatment solutions than other alkaline substrates. However, to our knowledge, no previous studies investigated the ability of biochar to adsorb P and F from PG leachates. Furthermore, the performance of biochar as a filter medium in passive treatment systems to absorb P and F from dynamic real PG leachate flows remains unknown.

This study aims to demonstrate the real-world application of biochar as a permeable reactive barrier packing material to treat P- and F-rich acidic solutions (i.e., PG leachates) to control P and F and improve water quality. Batch experiments were conducted to determine the adsorption characteristics and capacity of RHB for P and F from a real PG leachate solution. Dynamic adsorption experiments were performed to assess the effectiveness of biochar in treating P and F from PG leachates under different dosages and flow rates. Breakthrough models were used to examine the dynamic breakthrough behaviors in columns under different conditions. This study can be used as a guide for the effective and sustainable removal of P and F in leachates from PG piles worldwide.

Materials and Methods

Biochar Preparation

Rice husks, which are common and easily available agricultural residues in South China, were obtained from the rural areas of Chengdu, Sichuan Province, as biomass feedstock. According to our previous studies, the most effective RHB (RHB600) was pyrolyzed at 600 °C with a heating rate of 20 °C/min using a muffle furnace. The detailed biochar preparation process is presented in our previous study [16].

PG and PG Leachate Collection

The PG and PG leachate in this study were collected from one of the largest phosphate fertilizer factories in Shifang, China, which is one of the major areas of phosphate production. The leachate samples were collected daily at randomly selected times for 30 days. The PG leachate samples were filtered through 0.45-μm syringe filters to remove large suspended solids and stored at 4°C for further analysis.

The electrical conductance (EC) and pH of the leachate samples were measured by an EC and pH meter. The total phosphorus (TP) and aqueous F concentrations in the samples were determined using the Mo-Sb colorimetric method and the ion-selective electrode method, respectively [17-18]. The Pb, Zn, and Ca concentrations were measured via atomic absorption spectrometry (AAS) [19]. The parameters of the PG leachate samples were as follows: pH = 3.82 ± 0.65, EC = 3.74 ± 0.78 ms/cm, TP = 236.52 ± 68.05 mg/L, F = 79.64 ± 22.05, Ca = 426.65 ± 72.88 mg/L, Zn = 2.84 ± 0.57 mg/L, and Pb = 0.21 ± 0.04 mg/L.

Batch Experiments

Adsorption batch experiments were performed by mixing 50 ml of PG leachate with different solid/liquid ratios (e.g., 1:2, 1:4, 1:8, 1:10, and 1:20) with 3 g of RHB, according to our previous study [16], to measure the isotherms of the adsorption of P and F from the PG leachates onto the RHB. The mixture was placed in a 120-ml centrifuge tube and immediately shaken at room temperature and 250 rpm for 24 h. All batch experiments were conducted in triplicate. At the end of the experiments, the supernatant solutions were

centrifuged at 4500 rpm for 10 min, filtered through 0.45-μm syringe filters, and stored at 4 °C for analysis. Additional adsorption experiments were conducted with RHB via scanning electron microscopy with energy-dispersive X-ray spectroscopy (SEM-EDX) to explore the adsorption mechanism of the biochar. The biochar samples (1 g) were mixed with real PG leachate solutions (50 ml), which were shaken at 250 rpm for 24 h. After equilibration, biochar was obtained and dried in an oven at 105 °C for 24 h.

Column Experiment

A fixed-bed column experiment was conducted to measure the breakthrough curve (time-concentration profile) to determine the dynamic adsorption capacity of the adsorbent [20]. In this study, a Plexiglas column was used as a fixed-bed column and packed with RHB to evaluate the ability of RHB to adsorb P and F from real PG leachate. Different amounts (0, 12.65, 31, 62, and 93 g) of adsorbent (bulk density = 0.40 ± 0.003 g/cm^3) were packed in the columns at different bed heights (0, 2, 5, 10, and 15 cm) to determine the effects of the columns on the P and F removal. Different flow rates (1, 1.5, and 2 ml/min) were also used to identify the effect of the flow velocity on the dynamic removal of P and F. For each column, biochar was wet-packed with a moisture content of 5% (w/w) as an interlayer in a column, which was 300 mm in height, 45 mm in diameter, and 15.60 cm^2 in cross-sectional area. The top and bottom of each column were packed with washed quartz sand to sandwich and immobilize the biochar layer, which distributed the flow over the cross-sectional area. In addition, 75-μm nylon meshes were used to distribute the flow at the inlet of the column and stabilize the column content at the outlet of the column. A peristaltic pump was used to control the real PG leachate solutions and maintain a uniform flow rate of 0.5 ml/min through the columns from top to bottom. Effluent samples were collected from the bottom of the column during the experiments. All column experiments were conducted in duplicate. Six mathematical models, the Thomas, Yoon-Nelson, Adams-Bohart, Clark, modified dose–response, and bed depth service time (BDST) models were used to study the characteristics of the P and F experimental breakthrough curves under different conditions [21].

Results and Discussion

Sorption Isotherms

To evaluate the isothermal adsorption characteristics of the adsorbate–adsorbent interactions, experimental data were fitted by the Langmuir and the Freundlich models by varying the initial P and F concentrations from real PG leachates with different solid/liquid ratios. Fig. 1 shows the isotherms of the P and F adsorption from PG leachate on RHB, and Table 1 shows the corresponding fitting parameters. Langmuir model and Freundlich model showed different adsorption behaviors. The Langmuir model is commonly used to elucidate monolayer adsorption behaviors such as precipitation, whereas the Freundlich model is more applicable for multilayer adsorption behaviors such as electrostatic attraction [22]. For P, the Langmuir model (R^2 = 0.98) clearly fits the experimental data better than the Freundlich model (R^2 = 0.90). Therefore, the adsorption process of P from the PG leachate on RHB is mainly controlled by monolayer adsorption behaviors. The Langmuir maximum adsorption capacity (Q_{max}) of RHB for P from PG leachates was 3838 mg/kg. Although the Q_{max} value was lower than that reported in previous studies for many modified biochars with P in laboratory aqueous solutions, RHB could better remove P from PG leachates than other pristine biochars in removing P from aqueous solutions. These results indicate that RHB is more suitable for treating P from PG leachates than engineered biochars because of its low cost and lack of secondary pollution, specifically for large-area treatment. Conversely, the Freundlich model better described the adsorption of F from PG leachate on RHB (R^2 = 0.92) than the Langmuir model (R^2 = 0.90), which suggests that the F adsorption process on RHB is mainly dominated by multilayer adsorption. The Freundlich K_f value [446 (mg^{1-n}L^{n}kg^{-1})] for the F-isotherm model was larger than that for the P-isotherm model, which reflects the high F affinity of RHB.

SEM-EDX Analysis

Fig. 2 shows the SEM-associated EDX elemental dot maps of representative P and F from the PG leachates before and after adsorption by biochar. The khaki, dark red, bright red, cyan, transparent green, yellow, emerald green, and blue dots in the elemental maps of P- and

Table 1. Best-fit parameters of Langmuir and Freundlich isotherms for the adsorption of P and F.

Model	Item	Parameter 1	Parameter 2	R^2
Langmuir	P	K = 0.004	Q_{max} = 3838 (mg/kg)	0.98
	F	K = 0.29	Q_{max} = 2500 (mg/kg)	0.89
Freundlich	P	K_f = 99.81 (mg^{1-n}L^{n}kg^{-1})	n = 1.98	0.90
	F	K_f = 446 (mg^{1-n}L^{n}kg^{-1})	n = 1.14	0.92

Table 2. Parameters of six fixed-bed breakthrough models for the P and F adsorption onto RHB under different conditions via nonlinear regression analysis.

	Phosphorous							Fluoride						
Thomas	m (g)	Q (ml/min)	$k_{Th}\times10^{-2}$ (ml/mg/min)	q_m (mg/kg)	-	R^2	σ%	m (g)	Q (ml/min)	$k_{Th}\times10^{-2}$ (ml/mg/min)	q_m (mg/kg)	-	R^2	σ%
	12.65	0.500	2.23	8171	-	0.98	6.11	12.65	0.500	2.23	8171	-	0.98	6.11
	31.00	0.500	1.63	6396	-	0.98	5.21	31.00	0.500	1.63	6396	-	0.98	5.21
	62.00	0.500	1.34	5082	-	0.99	4.42	62.00	0.500	1.34	5082	-	0.99	4.42
	93.00	0.500	1.25	4924	-	0.99	2.23	93.00	0.500	1.25	4924	-	0.99	2.23
	12.65	1.000	2.44	10873	-	0.98	4.94	12.65	1.000	2.44	10873	-	0.98	4.94
	12.65	1.500	4.20	10009	-	0.98	5.14	12.65	1.500	4.20	10009	-	0.98	5.14
	12.65	2.000	5.76	9935	-	0.98	4.97	12.65	2.000	5.76	9935	-	0.98	4.97
Yoon-Nelson	m (g)	Q (ml/min)	k_{YN} (L/min)	λ_{cal} (min)	λ_{exp} (min)	R^2	σ%	m (g)	Q (ml/min)	k_{YN} (L/min)	λ_{cal} (min)	λ_{exp} (min)	R^2	σ%
	12.65	0.500	0.0129	464	452	0.96	10.44	12.65	0.500	0.0030	1614	1610	0.96	7.07
	31.00	0.500	0.0092	780	767	0.95	13.89	31.00	0.500	0.0021	3188	3206	0.98	5.36
	62.00	0.500	0.0053	1348	1350	0.95	14.45	62.00	0.500	0.0017	5037	5089	0.99	5.63
	93.00	0.500	0.0035	2089	2080	0.97	15.12	93.00	0.500	0.0016	7702	7691	0.99	2.46
	12.65	1.000	0.0182	209	192	0.95	10.24	12.65	1.000	0.0029	1146	1155	0.98	4.94
	12.65	1.500	0.0255	139	109	0.90	9.53	12.65	1.500	0.0050	702	653	0.98	5.13
	12.65	2.000	0.0694	83	79	0.96	8.40	12.65	2.000	0.0069	523	536	0.98	4.96
Adams-Bohart	h (cm)	v (cm/min)	$k_{AB}\times10^{-4}$ (ml/mg/min)	N_{AB} (mg/L)	-	R^2	σ%	h (cm)	v (cm/min)	$k_{AB}\times10^{-3}$ (ml/mg/min)	N_{AB} (mg/L)	-	R^2	σ%
	2.00	0.030	3.21	23872	-	0.27	22.41	2.00	0.030	4.16	6750	-	0.72	19.74
	5.00	0.030	4.28	10405	-	0.37	28.08	5.00	0.030	3.02	4883	-	0.78	17.74
	10.00	0.030	6.13	5681	-	0.54	25.50	10.00	0.030	3.81	2703	-	0.83	14.12
	15.00	0.030	6.26	4254	-	0.55	24.04	15.00	0.030	9.74	1987	-	0.98	3.12
	2.00	0.060	6.09	29200	-	0.39	22.41	2.00	0.060	4.88	8774	-	0.77	15.84
	2.00	0.095	4.12	45399	-	0.25	22.22	2.00	0.095	7.95	8852	-	0.71	17.30
	2.00	0.126	8.52	35822	-	0.31	23.43	2.00	0.126	11.71	8353	-	0.74	16.23

	Phosphorous							Fluoride						
Clark	m (g)	Q (ml/min)	k	r (min^{-1})	-	R^2	σ%	m (g)	Q (ml/min)	k	r (min^{-1})	-	R^2	σ%
	12.65	0.500	181.13	0.011	-	0.95	10.23	12.65	0.500	2.37	0.0019	-	0.99	4.21
	31.00	0.500	445.43	0.007	-	0.93	13.80	31.00	0.500	7.51	0.0013	-	0.99	3.95
	62.00	0.500	101.47	0.003	-	0.92	12.85	62.00	0.500	37.63	0.0011	-	0.99	3.07
	93.00	0.500	327.92	0.002	-	0.93	12.89	93.00	0.500	457.42	0.0011	-	0.99	1.58
	12.65	1.000	42.71	0.018	-	0.95	10.23	12.65	1.000	1.20	0.0022	-	0.99	3.08
	12.65	1.500	80.29	0.025	-	0.90	9.52	12.65	1.500	1.25	0.0036	-	0.99	3.15
	12.65	2.000	293.43	0.068	-	0.96	8.38	12.65	2.000	1.35	0.0051	-	0.99	3.01
Modified dose–response	m (g)	Q (ml/min)	q_m (mg/kg)	β	-	R^2	σ%	m (g)	Q (ml/min)	q_m (mg/kg)	β		R^2	σ%
	12.65	0.500	5935	3.68	-	0.95	8.76	12.65	0.500	5935	3.68	-	0.95	8.76
	31.00	0.500	4150	3.65	-	0.91	11.93	31.00	0.500	4150	3.65	-	0.91	11.93
	62.00	0.500	3813	3.55	-	0.93	10.40	62.00	0.500	3813	3.55	-	0.93	10.40
	93.00	0.500	3833	4.46	-	0.93	10.97	93.00	0.500	3833	4.46	-	0.93	10.97
	12.65	1.000	5183	2.32	-	0.94	8.57	12.65	1.000	10297	3.32	-	0.99	2.11
	12.65	1.500	4605	2.40	-	0.93	7.43	12.65	1.500	9589	3.27	-	0.99	1.82
	12.65	2.000	3962	4.73	-	0.96	7.61	12.65	2.000	9534	3.40	-	0.99	1.88
BDST	Relationship	Breakthrough point (C_e/C_0)	$k_B\times10^{-2}$ (ml/mg/min)	q_0 (mg/L)	-	R^2	-	Relationship	Breakthrough point (C_e/C_0)	$k_B\times10^{-2}$ (ml/mg/min)	q_0 (mg/L)	-	R^2	-
	Dosage	0.6	0.86	1144	-	0.98	-	Dosage	0.6	0.98	2788	-	0.99	-
		0.7	2.67	1540	-	0.99	-		0.7	1.99	3606	-	0.99	-
		0.8	6.38	2339	-	0.91	-		0.8	3.33	5050	-	0.99	-
	Flow rate	0.6	-2.51	143	-	0.99	-	Flow rate	0.6	2.20	138	-	0.99	-
		0.7	-7.67	469	-	0.97	-		0.7	3.06	228	-	0.97	-
		0.8	25.60	777		0.97	-		0.8	4.27	383	-	0.98	-

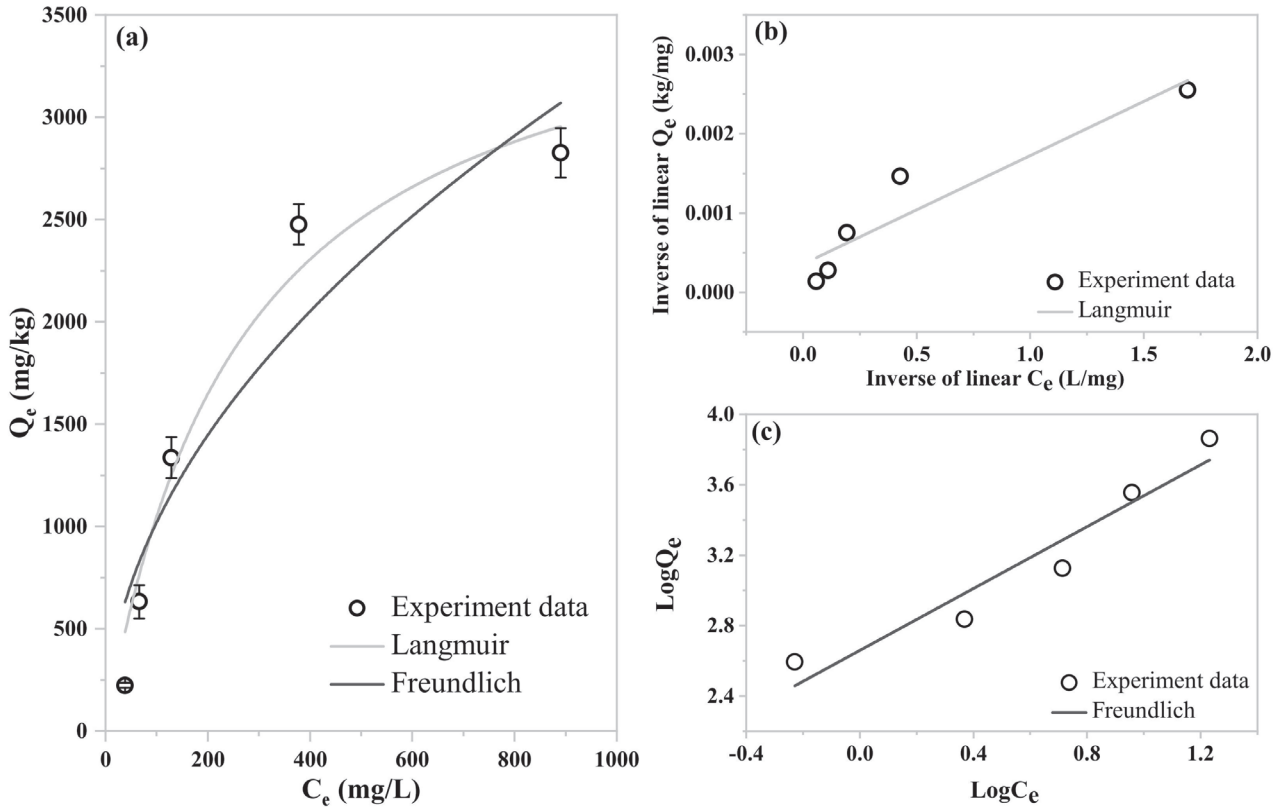

Fig. 1. Adsorption isotherms of RHB for (a) P and (b) and (c) F adsorption from PG leachate. The results are shown as averages and standard deviations (n=3). The lines represent the model fittings.

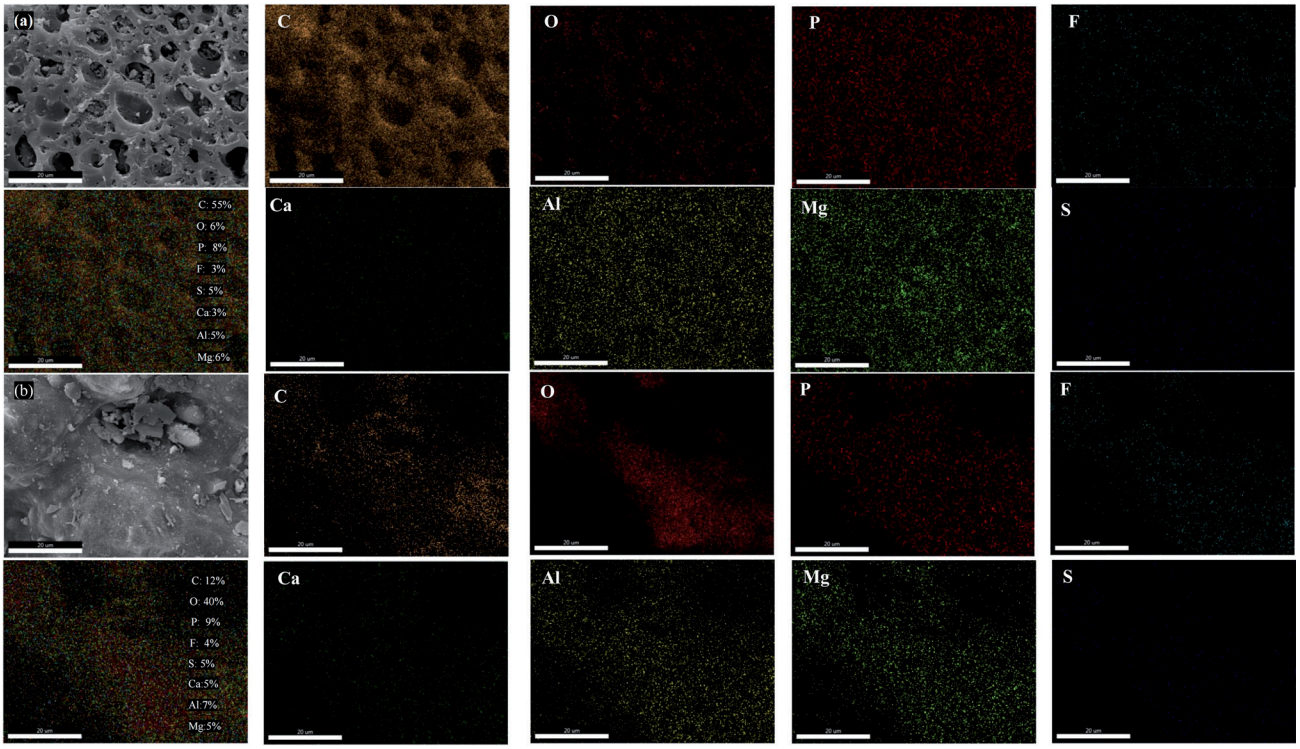

Fig. 2. Scanning electron microscopy (SEM) images and energy-dispersive X-ray spectroscopy (EDX) elemental dot maps of RHB before (a) and after (b) adsorption. Elemental dot maps of C (khaki), O (dark red), P (bright red), F (cyan), Ca (transparent green), Al (yellow), Mg (emerald green) and S (blue) dots, which denote the C, O, P, F, Ca, Al, Mg and S concentrations, are mainly associated with the adsorption of P and F.

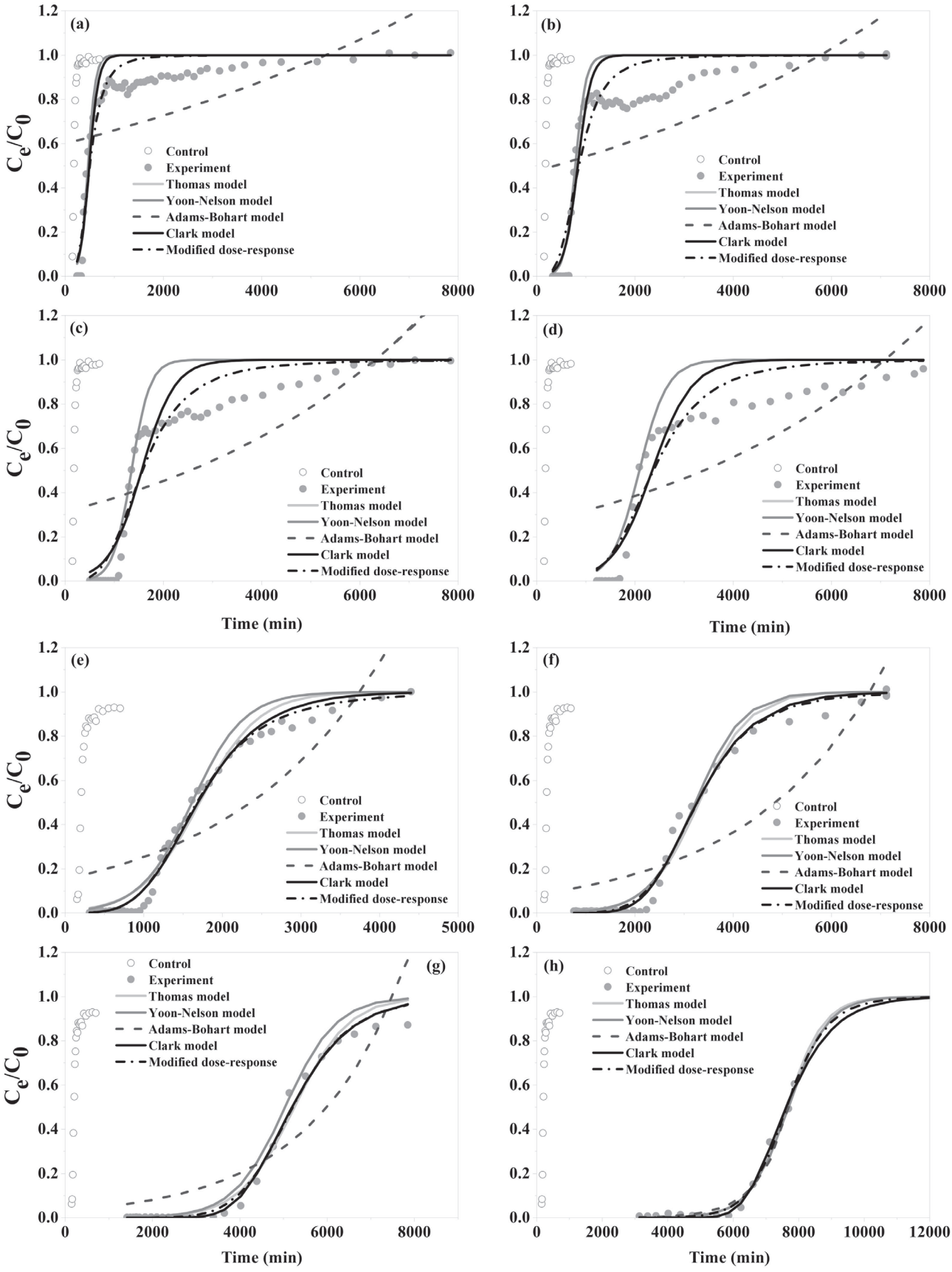

Fig. 3. Breakthrough curves of P [(a), (b), (c) and (d)] and F [(e), (f), (g) and (h)] from PG leachate with an RHB-packed column at different dosages (bed heights): (a), (e) 12.65 g; (b), (f) 31 g; (c), (g) 62 g; (d), (h) 93 g. The breakthrough curves were fitted with five different breakthrough models. The experimental data (solid grey circles) were simulated with various models.

F-loaded biochar samples denote the concentrations of C, O, P, F, Ca, Al, Mg, and S, respectively. The EDX elemental mapping results show that C, O, Al, and Mg were the major elements in the biochar structure. However, the intensity and brightness of O on the biochar surface in the elemental maps increased after adsorption due to the phosphate adsorption on the biochar [23]. Importantly, the intensities of P, F, Ca, and Al in the elemental maps increased after the adsorption, which confirms that P, F, and metals were absorbed by the biochar. The brightness and distribution outlines of the bright red and cyan dots in the elemental maps of P and F were associated with those of the khaki (C), transparent green (Ca), yellow (Al), and emerald green (Mg) dots in the maps, which indicates a correlation among the adsorption of P and F and the basic elements C, Ca, Al, and Mg. The elemental map data may indicate that the process of P and F adsorption can be divided into two steps: first, metal ions (Ca, Al, and Mg) from the PG leachates were absorbed on the biochar through electrostatic attraction and complexation [24]; second, the absorbed metal ions acted as bridges to precipitate P and F from the PG leachates, which made relatively insoluble Ca/Mg-P, Ca/Mg-F, or Al-F compounds immobilize P and F in the biochar [25-26]. However, C- and O-containing surface functional groups could also contribute to the adsorption of P and F from leachates onto the biochar surface through ion exchange, electrostatic interactions, or surface precipitation [27], although the correlation between P and O in the elemental maps was not significant due to the impact of endogenous phosphorus in biochar. In addition, our elemental dot maps revealed the presence of S in the biochar, and the intensity and brightness of S did not obviously change before and after adsorption, which indicates that sulfate ions did not significantly affect the adsorption of P and F from PG leachates by the biochar.

Fixed-bed Column Adsorption of P and F from PG Leachates

Effects of the Biochar Dosage

Fig. 3 shows the effects of different biochar dosages on the column adsorption of P and F from PG leachates. Four biochar dosages (12.65, 31, 62, and 93 g) were used to establish the column adsorbent layer. The results revealed much lower P and F concentrations in the effluents of all four biochar columns than in the control (i.e., a column filled with only sand), which indicates immediate P and F breakthrough, i.e., RHB in the fixed-bed columns can positively remove P and F from PG leachates. However, the breakthrough curves of P and F had considerably different profiles. The slope of each breakthrough curve of P markedly changed from high to low during the adsorption process, possibly because a transition to an interparticle control mechanism caused the diffusion in macro/micropores or surface reaction kinetics [28]. In addition, the slopes of the P and F breakthrough curves decreased with increasing biochar dosage due to a greater mass transfer zone. The contact time between PG leachates and RHB increased with increasing adsorbent dosage (bed height), which increased the P and F removal and decreased the slope of the breakthrough curves. Moreover, the surface area in the packed layer in the column increased with increasing adsorbent bed height, which contributed to the formation of adsorption sites on RHB to adsorb P and F.

The performance of RHB in fixed-bed columns can simulate real-life applications in P and F removal for PG leachate treatment. The breakthrough curve models (Thomas, Yoon-Nelson, Adams-Bohart, Clark, and the modified dose–response models) were used for the practical design of fixed-bed filters. All experimental data were fitted by these models, and Table 2 lists the corresponding fitting parameters. The model fitting results show that although the experimental breakthrough curves were well fitted by all models (except the Adams-Bohart model), overall, all model simulations better fit the F experimental breakthrough curves than the P experimental breakthrough curves. The Adams-Bohart model had the worst fit to the experimental curves because it was only applied to the initial phase (approximately 50% concentration) of the breakthrough curves [21]. Hence, the performance of the F breakthrough curve at a bed height of 15 cm fitted by the Adams-Bohart model was very good (R^2 = 0.98; $\sigma\%$ = 3.12). For P, the Yoon-Nelson model exhibited the best fit because of the higher R^2 value ($R^2 > 0.95$) with average $\sigma\%$ among all models. The values of k_{YN} and λ of the Yoon-Nelson model decreased and increased with increasing bed height, respectively, because the increased contact time increased the adsorbate breakthrough time. Similarly, the parameter values of the Thomas model and the modified dose–response model decreased with increasing bed height, which indicates that external and internal diffusion is not the limiting step [29]. In contrast, the Clark model exhibited the best fit to the F breakthrough curve at different adsorbent dosages with an average R^2 = 0.99 and the lowest $\sigma\%$. The rate of mass transfer decreased with increasing bed height (dosage) because of the increased interactions between RHB adsorbent and F from the PG leachates with increasing adsorbent dosage, which reduced the mass transfer rate [30].

In addition, the BDST model was used to evaluate the effect of dosage on P and F removal by RHB in fixed-bed columns. The BDST model was applied to the breakthrough point at effluent and influent concentration ratios of C_e/C_0 = 0.6, 0.7, and 0.8, as shown in Fig. 4. The results indicate that the contact time at a certain effluent and influent concentration ratio increased with increasing bed height. Table 2 lists the best-fit model parameters. For P and F, the dynamic adsorption capacities obtained via BDST model fitting increased with increasing C_e/C_0 because P and F occupied more RHB active sites at higher C_e/C_0 values, which improved

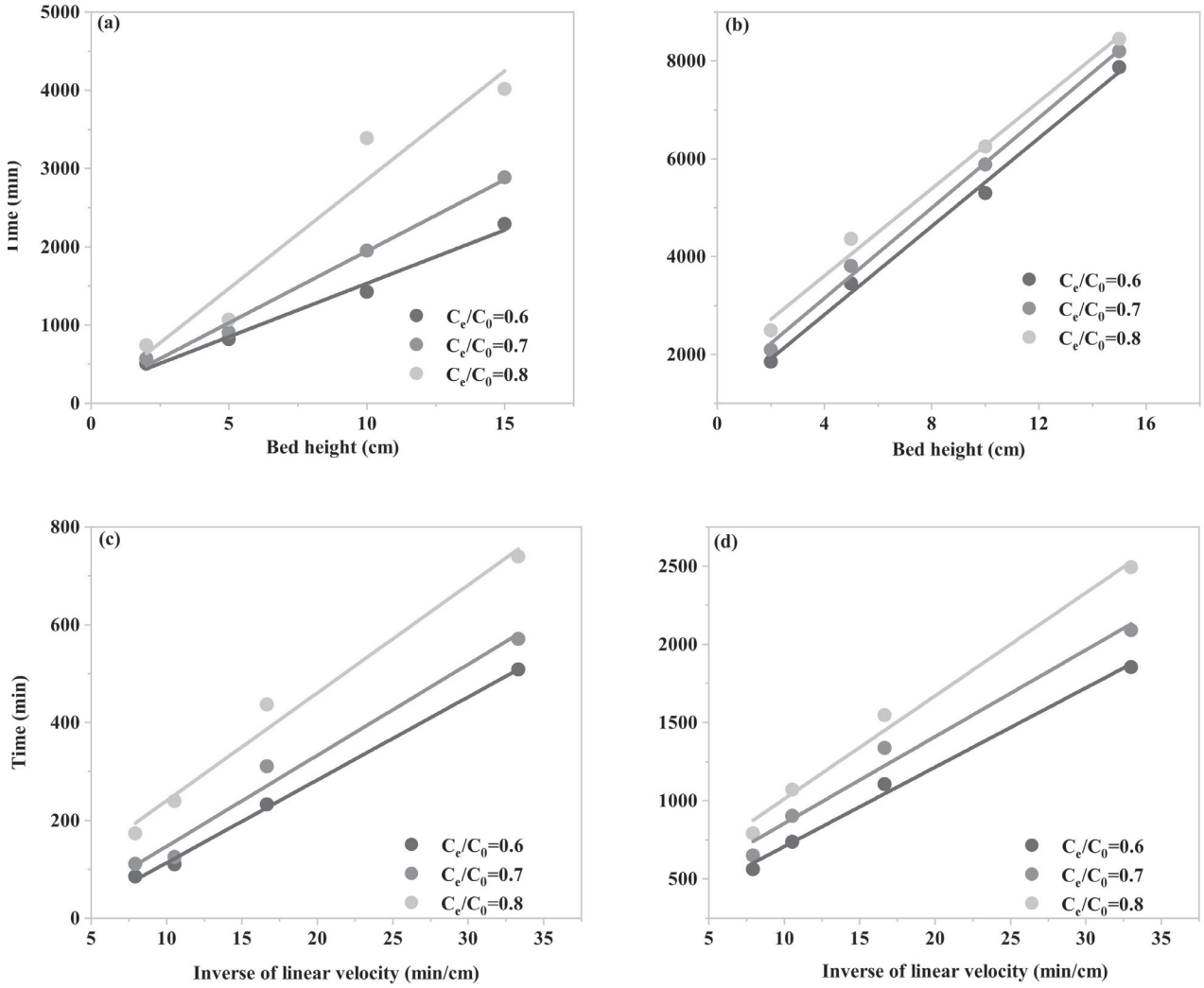

Fig. 4 BDST model linear regression between the bed height (cm) [P (a) and F (b)] and the inverse of the linear velocity (min/cm) [P (c) and F (b)] and service time (min) at breakthrough points of C_e/C_0 = 0.6, 0.7 and 0.8.

the adsorption capacity [31]. Moreover, according to the fitting results of q_0 (mg/L), RHB could remove more F than P under identical conditions. Therefore, it is feasible to use the BDST model to predict the operation of a fixed bed in a certain range of conditions, which has guiding significance for selecting the conditions for the practical application of RHB treatment of PG leachates on a large scale.

Effect of the Flow Rate

Fig. 5 shows the effects of different flow rates (0.5, 1, 1.5, and 2 ml/min) on the dynamic removal of P and F from PG leachates using a column with an RHB dosage of 12.65 g (i.e., a bed height of 2 cm). In all flow rate experiments, the biochar column significantly affected the removal of P and F from the PG leachates, which indicates the effectiveness of RHB in treating P and F from real PG leachates. However, increasing the flow rate shortened the breakthrough time by reducing the contact time between P and F in the PG leachates and RHB in the column. At the lowest flow rate, the longest breakthrough times were 361 and 1113 min for P and F, respectively. In contrast, at the highest flow rate, the shortest breakthrough times were 63 and 285 min. These results indicate that a high flow rate can shorten the residence time of PG in the column and limit the exposure of P and F from PG leachates to RHB [32].

The five breakthrough curve models also fit the experimental data on the dynamic adsorption of P and F from PG leachates well. The models better fitted the flow rate data with higher R^2 and lower $\sigma\%$ values than the dosage data as shown in Table 2. Furthermore, the dynamic adsorption capacity q_m of the Thomas model and the modified dose–response models gradually decreased for both P and F with increasing flow rate. As previously mentioned, this reduction is likely attributed to the decreased residence time of the PG leachates and limited contact time. However, with increasing flow rate, k_{YN} and λ of the Yoon-Nelson model increased and decreased, respectively, contrary to the increasing trend of dosage. Similarly, the excellent fitting quality

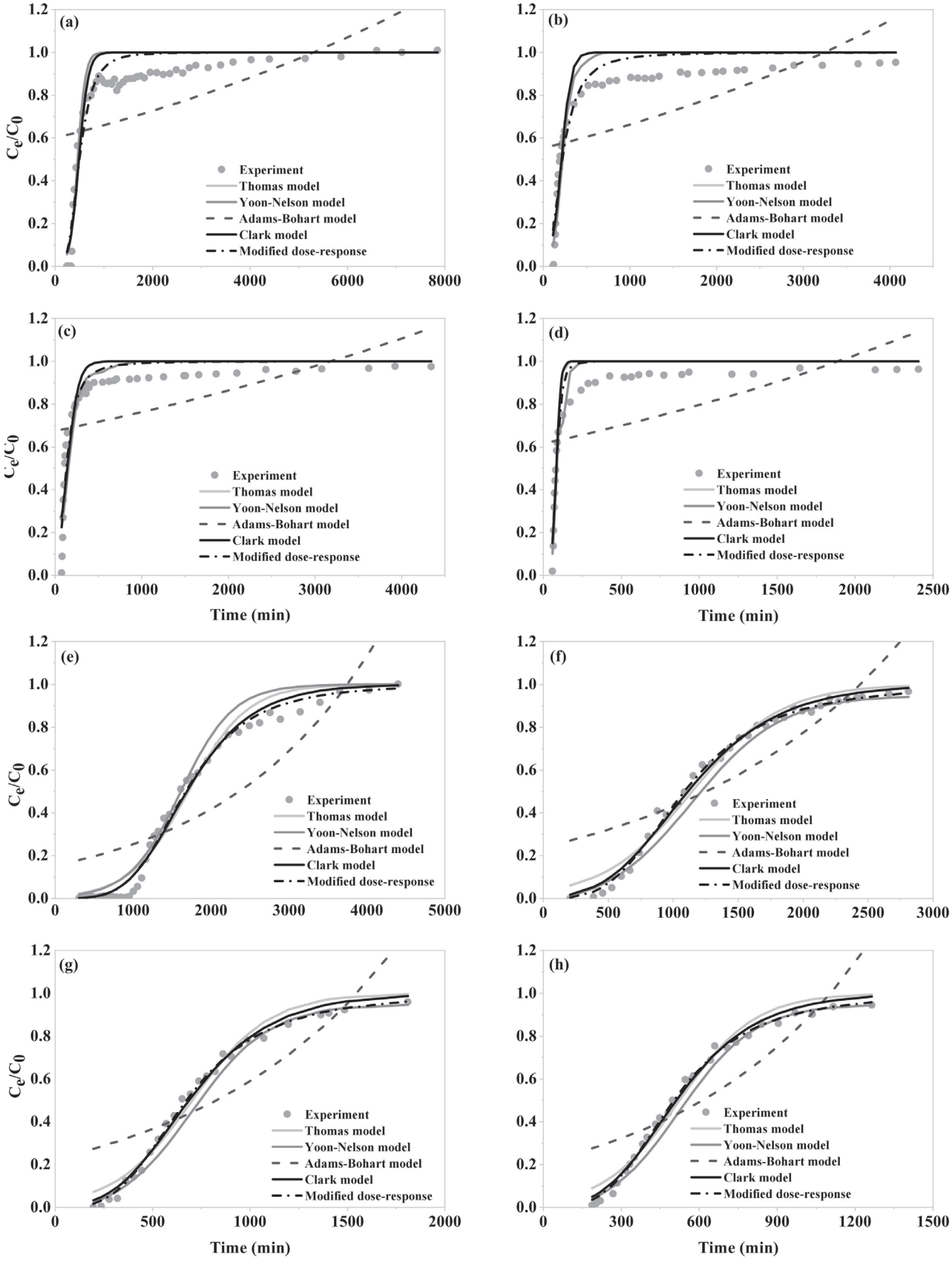

Fig. 5. Breakthrough curves of P [(a), (b), (c) and (d)] and F [(e), (f), (g) and (h)] from PG leachate with an RHB-packed column at a dosage of 12.65 g and different flow rates: (a), (e) 0.5 ml/min; (b), (f) 1 ml/min; (c), (g) 1.5 ml/min; (d), (h) 2 ml/min. The breakthrough curves were fitted with five different breakthrough models. The experimental data (solid grey circles) were simulated with various models.

of the Clark model for F might result from the batch adsorption process following the Freundlich model and a high degree of mass transfer during the entire process in the column [33]. The corresponding breakthrough points were fitted by the BDST model in Fig. 4, and the model well-fitted the linear relationship between the service time and the reverse of the linear velocity (Table 2; $R^2 > 0.98$ for P and F). Consistently, the fitting results of q_0 increased with increasing C_e/C_0, which confirms that RHB was successfully applied as a packing material to remove P and F from PG leachates.

Conclusions

In summary, this study provides a low-cost and safe material to remove P and F from real acidic PG solutions, although biochar has been used to decrease or immobilize heavy metals in aqueous solutions or soil, and modified biochar has been used to adsorb P or F from aqueous solutions. The P and F concentrations of the PG leachates significantly decreased with the addition of biochar, which prevented secondary pollution and modified the costs to the maximum extent. Batch adsorption experiments were performed to investigate the adsorption characteristics and capacity of RHB, and the results indicated that RHB had good P and F adsorption capacity for the PG leachates. The physicochemical properties and isotherm models revealed that the main mechanisms in the adsorption of P and F were likely electrostatic interactions and precipitation through a "metal bridge". Compared with the observed P and F removal in the control experiment, different dosages of RHB packed in a column significantly affected the removal of P and F from PG leachates. All RHB dosages and flow rates of influent had excellent effects on the P and F removal. Furthermore, five common dynamic adsorption models were used to describe the P and F breakthrough behaviors in the columns well. Among all breakthrough models, the Yoon-Nelson and Clark models best described the experimental data for P and F under different conditions with the highest R^2 and lowest $\sigma\%$ values. The BDST model revealed a strong linear relationship between the bed height and the reverse relationship between linear velocity and service time, which indicates that the use of RHB as a packing material in fixed-bed columns has promising potential for treating P and F from PG leachates. These findings suggest that RHB may be a reliable absorbent to remove P and F and can be used for real acid PG leachate treatment in large-scale applications. Further research is necessary to explore the potential reclamation of P from the P-rich acidic solution of this material to sequester carbon and improve P cycling in the environment.

Acknowledgements

This work was financially supported by the Open Fund of Sichuan Provincial Engineering Research Center of City Solid Waste Energy and Building Materials Conversion and Utilization Technology (No. GF2024ZC06), the Science & Technology Department of Chengdu (2022-YF05-00561-SN), and the Scientific Research Foundation of Talent of Chengdu University (No. 2081921088).

Competing Interests

The authors declare that they have no conflicts of interest.

References

1. SILVA L.F., OLIVEIRA M.L., CRISSIEN T.J., SANTOSH M., BOLIVAR J., SHAO L., DOTTO G.L., GASPAROTTO J., SCHINDLER M. A review on the environmental impact of phosphogypsum and potential health impacts through the release of nanoparticles. Chemosphere, **286**, 131513, **2022**.
2. PENG X., DENG Y., ZHANG X., LIU L., HU J., DUAN X., WEI Z., FENG Q., SHEN K. The leaching characteristics of common toxic elements in phosphogypsum. Geochemistry: Exploration, Environment, Analysis, **20** (4), 473, **2020**.
3. CONLEY D.J., PAERL H.W., HOWARTH R.W., BOESCH D.F., SEITZINGER S.P., HAVENS K.E., LANCELOT C., LIKENS G.E. Controlling eutrophication: nitrogen and phosphorus. Science, **323** (5917), 1014, **2009**.
4. HUANG Y., CIAIS P., GOLL D.S., SARDANS J., PEñUELAS J., CRESTO-ALEINA F., ZHANG H. The shift of phosphorus transfers in global fisheries and aquaculture. Nature Communications, **11** (1), 355, **2020**.
5. SHI Y., QIN Y.W., MA Y.-Q., ZHAO Y.M., WEN Q., CAO W., QIAO F. Pollution Status and Control Strategy of 'Three Phosphorus' Pollution in the Upper Reaches of Yangtze River Basin, China. Research of Environmental Sciences, **33** (10), 2283, **2020** [In Chinese].
6. QIN Y., MA Y., WANG L., ZHENG B., REN C., TONG H., WANG H. Pollution of the total phosphorus in Yangtze river Basin: distribution characteristics, source and control strategy. Research of Environmental Sciences, **31** (1), 9, **2018** [In Chinese].
7. YADAV K.K., KUMAR S., PHAM Q.B., GUPTA N., REZANIA S., KAMYAB H., YADAV S., VYMAZAL J., KUMAR V., TRI D.Q. Fluoride contamination, health problems and remediation methods in Asian groundwater: A comprehensive review. Ecotoxicology and Environmental Safety, **182**, 109362, **2019**.
8. DEHGHANI M.H., FARHANG M., ALIMOHAMMADI M., AFSHARNIA M., MCKAY G. Adsorptive removal of fluoride from water by activated carbon derived from CaCl2-modified Crocus sativus leaves: Equilibrium adsorption isotherms, optimization, and influence of anions. Chemical Engineering Communications, **205** (7), 955, **2018**.
9. SHAJI E., SARATH K., SANTOSH M.,

KRISHNAPRASAD P., ARYA B., BABU M.S. Fluoride contamination in groundwater: A global review of the status, processes, challenges, and remedial measures. Geoscience Frontiers, **15** (2), 101734, **2024**.
10. WEIKSNAR K.D., CLAVIER K.A., LAUX S.J., TOWNSEND T.G. Influence of trace chemical constituents in phosphogypsum for road base applications: A review. Resources, Conservation and Recycling, **199**, 107237, **2023**.
11. GUERRERO J.L., GUTIéRREZ-ÁLVAREZ I., MOSQUEDA F., OLíAS M., GARCíA-TENORIO R., BOLíVAR J.P. Pollution evaluation on the salt-marshes under the phosphogypsum stacks of Huelva due to deep leachates. Chemosphere, **230,** 219, **2019**.
12. MILLáN-BECERRO R., PéREZ-LóPEZ R., MACíAS F., CáNOVAS C.R. Design and optimization of sustainable passive treatment systems for phosphogypsum leachates in an orphan disposal site. Journal of Environmental Management, **275**, 111251, **2020**.
13. WANG L., O'CONNOR D., RINKLEBE J.R., OK Y.S., TSANG D.C., SHEN Z., HOU D. Biochar aging: mechanisms, physicochemical changes, assessment, and implications for field applications. Environmental Science & Technology, **54** (23), 14797, **2020**.
14. LIU T., LAWLUVY Y., SHI Y., IGHALO J.O., HE Y., ZHANG Y., YAP P.-S. Adsorption of cadmium and lead from aqueous solution using modified biochar: A review. Journal of Environmental Chemical Engineering, **10** (1), 106502, **2022**.
15. JOSEPH S., COWIE A.L., VAN ZWIETEN L., BOLAN N., BUDAI A., BUSS W., CAYUELA M.L., GRABER E.R., IPPOLITO J.A., KUZYAKOV Y. How biochar works, and when it doesn't: A review of mechanisms controlling soil and plant responses to biochar. Global Change Biology Bioenergy, **13** (11), 1731, **2021**.
16. PENG X., DENG Y., LIU L., TIAN X., GANG S., WEI Z., ZHANG X., YUE K. The addition of biochar as a fertilizer supplement for the attenuation of potentially toxic elements in phosphogypsum-amended soil. Journal of Cleaner Production, **277**, 124052, **2020**.
17. AKHTAR K., WANG W., REN G., KHAN A., FENG Y., YANG G. Changes in soil enzymes, soil properties, and maize crop productivity under wheat straw mulching in Guanzhong, China. Soil and Tillage Research, **182**, 94, **2018**.
18. YU K., WANG Q., XIANG W., LI Z., HE Y., ZHAO D. Amino-functionalized single-lanthanide metal–organic framework as a ratiometric fluorescent sensor for quantitative visual detection of fluoride ions. Inorganic Chemistry, **61** (34), 13627, **2022**.
19. AYDIN F., ÇAKMAK R., LEVENT A., SOYLAK M. Silica Gel-Immobilized 5-aminoisophthalohydrazide: A novel sorbent for solid phase extraction of Cu, Zn and Pb from natural water samples. Applied Organometallic Chemistry, **34** (4), e5481, **2020**.
20. AMEN R., BASHIR H., BIBI I., SHAHEEN S.M., NIAZI N.K., SHAHID M., HUSSAIN M.M., ANTONIADIS V., SHAKOOR M.B., AL-SOLAIMANI S.G. A critical review on arsenic removal from water using biochar-based sorbents: the significance of modification and redox reactions. Chemical Engineering Journal, **396**, 125195, **2020**.
21. ZHENG Y., WANG B., WESTER A.E., CHEN J., HE F., CHEN H., GAO B. Reclaiming phosphorus from secondary treated municipal wastewater with engineered biochar. Chemical Engineering Journal, **362**, 460, **2019**.
22. ZHOU L., RICHARD C., FERRONATO C., CHOVELON J.M., SLEIMAN M. Investigating the performance of biomass-derived biochars for the removal of gaseous ozone, adsorbed nitrate and aqueous bisphenol A. Chemical Engineering Journal, **334**, 2098, **2018**.
23. YU J., LI X., WU M., LIN K., XU L., ZENG T., SHI H., ZHANG M. Synergistic role of inherent calcium and iron minerals in paper mill sludge biochar for phosphate adsorption. Science of the Total Environment, **834**, 155193, **2022**.
24. BANDARA T., XU J., POTTER I.D., FRANKS A., CHATHURIKA J., TANG C. Mechanisms for the removal of Cd (II) and Cu (II) from aqueous solution and mine water by biochars derived from agricultural wastes. Chemosphere, **254**, 126745, **2020**.
25. ADUSEI-GYAMFI J., OUDDANE B., RIETVELD L., CORNARD J.-P., CRIQUET J. Natural organic matter-cations complexation and its impact on water treatment: A critical review. Water Research, **160**, 130, **2019**.
26. XIAO X., CHEN B., CHEN Z., ZHU L., SCHNOOR J.L. Insight into multiple and multilevel structures of biochars and their potential environmental applications: a critical review. Environmental Science & Technology, **52** (9), 5027, **2018**.
27. ZHANG M., SONG G., GELARDI D.L., HUANG L., KHAN E., MAŠEK O., PARIKH S.J., OK Y.S. Evaluating biochar and its modifications for the removal of ammonium, nitrate, and phosphate in water. Water Research, **186**, 116303, **2020**.
28. SINHA R., KUMAR R., SHARMA P., KANT N., SHANG J., AMINABHAVI T.M. Removal of hexavalent chromium via biochar-based adsorbents: State-of-the-art, challenges, and future perspectives. Journal of Environmental Management, **317**, 115356, **2022**.
29. KHASRI A., AHMAD M.A. Adsorption of basic and reactive dyes from aqueous solution onto Intsia bijuga sawdust-based activated carbon: batch and column study. Environmental Science and Pollution Research, **25** (31), 31508, **2018**.
30. HASHEM A., BADAWY S., FARAG S., MOHAMED L., FLETCHER A., TAHA G. Non-linear adsorption characteristics of modified pine wood sawdust optimised for adsorption of Cd (II) from aqueous systems. Journal of Environmental Chemical Engineering, **8** (4), 103966, **2020**.
31. MAIA M.A., DOTTO G.L., PEREZ-LOPEZ O.W., GUTTERRES M. Phosphate removal from industrial wastewaters using layered double hydroxides. Environmental Technology, **42** (20), 3095, **2021**.
32. HUANG J., ZIMMERMAN A.R., CHEN H., WAN Y., ZHENG Y., YANG Y., ZHANG Y., GAO B. Fixed bed column performance of Al-modified biochar for the removal of sulfamethoxazole and sulfapyridine antibiotics from wastewater. Chemosphere, **305**, 135475, **2022**.
33. HU Q., LIU H., ZHANG Z., PEI X. Development of fractal-like Clark model in a fixed-bed column. Separation and Purification Technology, **251**, 117396, **2020**.